Physics Letters A 383 (2019) 1907–1914

Contents lists available at ScienceDirect

Physics Letters A

www.elsevier.com/locate/pla

Stabilization of Lagrange points in circular restricted three-body problem: A port-Hamiltonian approach

Chang Liu [a,b,*], Lu Dong [b]

[a] Johns Hopkins University, 3400 N. Charles Street, Baltimore, MD, 21218, USA
[b] Shanghai Jiao Tong University, Dongchuan Road 800, Shanghai, 200240, China

ARTICLE INFO

Article history:
Received 17 December 2018
Received in revised form 5 February 2019
Accepted 25 March 2019
Available online 29 March 2019
Communicated by F. Porcelli

Keywords:
Lagrange points
Circular Restricted Three-Body Problem
Port-Hamiltonian
Global stability

ABSTRACT

Current station keeping strategies target periodic orbits around the unstable Lagrange points. These control strategies are based on the Circular Restricted Three-Body Problem (CRTBP) linearized around an equilibrium point and cannot ensure global stability. In this paper, we use the port-Hamiltonian approach to reformulate the CRTBP with input, which preserves the original nonlinear dynamics. Designing a control strategy based on energy shaping and dissipation injection, we obtain the closed-loop Hamiltonian as the candidate of Lyapunov function, which guarantees asymptotic stability. The control strategy designed here is successfully applied to the stabilization of Lagrange points in CRTBP. Furthermore, the designed control approach shows global stability within the application region of CRTBP model, and it is applicable to set arbitrary equilibrium points. The current framework is also stable against error in the thrust and still works when the third body moves beyond the region of applicability of the linearized dynamics, where the linear controller may fail. Finally, this method has potential to be extended to the three-dimensional CRTBP, where both the perturbation and the thrust out of the plane are considered.

1. Introduction

The Circular Restricted Three-Body Problem (CRTBP) [1,2] has been examined for over 300 years. It has been widely used in the last few decades to model the Earth-Moon system with a spacecraft in determining spacecraft orbital maneuvers required for missions to the Moon. The CRTBP is also used to investigate the Sun-Earth-Moon system and to determine the stability conditions [3–6].

Lagrange studied the CRTBP and demonstrated that there were five equilibrium points (Lagrange points or Libration points) where the gravitational forces of these bodies balanced out. The Lagrange points are of much importance in science and engineering. For example, discovered in 1906, the Trojan asteroids along Jupiter's orbit are located at a region close to two of the Lagrange points. Furthermore, a remote sensor orbiting around a Sun-Earth Lagrange point will rotate around the Sun at the same angular speed as the Earth. Attributed to its high distance from the Earth, the space environment around a Lagrange point undergoes few perturbations and is thus appealing for various scientific applications. Among them, the creation of virtual telescopes to observe celestial objects with an unprecedented precision is one of the most promising projects; e.g., artificial spacecrafts have been placed at the L_1 and L_2 Lagrange points with respect to the Sun and the Earth [7–10] and Lagrange points with respect to the Earth and the Moon [11,12].

However, these are also the most challenging projects because the L_1, L_2 and L_3 Lagrange points are unstable [1,13]. There exist, fortunately, stable orbits called Halo orbits [14,15] around the unstable Lagrange points, which are used to park the artificial spacecraft. Current frameworks of station keeping on the Halo orbit are based on the restricted three-body equations linearized around the Lagrange point [16–18]. Halo orbits can also be generated around these Lagrange points by selecting suitable initial conditions that result in periodic solutions of the linearized three-body equations [17]. With respect to the nonlinear dynamics, the Fourier series approximation and the nonlinear output regulation method have recently been applied on the halo orbit of the Sun-Earth L_2 point [19].

Stability analysis based on the linearized three-body equations only guarantees that the system is stable to infinitesimal perturbations, but it may be unstable to finite ones. Perturbations for the Earth-Moon Lagrange points mission under the CRTBP model include the eccentricity of the Earth-Moon orbit, the gravity from the other bodies [20] and the solar radiation pressure. For the Sun-

* Corresponding author at: Johns Hopkins University, 3400 N. Charles Street, Baltimore, MD, 21218, USA.
E-mail address: changliu@jhu.edu (C. Liu).

https://doi.org/10.1016/j.physleta.2019.03.033
0375-9601/

Earth Lagrange points mission, the perturbation from the Moon is critical. Over a century ago, Lyapunov [21] generalized the notions of stability to nonlinear dynamics [22]. Lyapunov's second method for stability considers the system $\dot{\boldsymbol{x}} = \boldsymbol{f}(\boldsymbol{x})$ with an equilibrium $\boldsymbol{x} = \boldsymbol{x}^*$. If there exists a Lyapunov function $V(\boldsymbol{x})$ satisfying:

$$\begin{aligned} &V(\boldsymbol{x}) = 0, \ \ \boldsymbol{x} = \boldsymbol{x}^* \\ &V(\boldsymbol{x}) > 0, \ \ \forall \boldsymbol{x} \neq \boldsymbol{x}^* \\ &\frac{dV(\boldsymbol{x})}{dt} = \nabla_{\boldsymbol{x}} V(\boldsymbol{x}) \dot{\boldsymbol{x}} = \nabla_{\boldsymbol{x}} V(\boldsymbol{x}) \boldsymbol{f}(\boldsymbol{x}) \leq 0, \ \ \forall \boldsymbol{x} \neq \boldsymbol{x}^*, \end{aligned} \tag{1}$$

then the system is stable in the sense of Lyapunov. Moreover, if $\frac{dV(\boldsymbol{x})}{dt} < 0, \ \forall \boldsymbol{x} \neq \boldsymbol{x}^*$, then the system is asymptotically stable. Lyapunov stability analysis was initially used to analyze the restricted three-body problem [23] but Lyapunov-based control [24] for the CRTBP is not broached in detail. In the Lyapunov stability analysis and the Lyapunov-based control, the major difficulty is to find the Lyapunov function $V(\boldsymbol{x})$.

For a Hamiltonian system, the Hamiltonian is a natural candidate for the Lyapunov function. Another important contribution to the CRTBP was made by Jacobi [25], who used the synodic (rotating) coordinate system originally introduced by Euler [26] to demonstrate that there was an integral of motion, which is now named the Jacobi integral. The Jacobi integral allows us to formulate and analyze the CRTBP using a Hamiltonian framework.

The port-Hamiltonian framework [27] extends the formalism of a Hamiltonian system to include input and dissipation, which are described as 'port'. This framework has the potential to model, analyze, and especially, control complex physical systems and their interconnections [28]. The port-Hamiltonian framework also provides a physics-based control strategy [29–32], which focuses on shaping the closed-loop Hamiltonian as the candidate of Lyapunov function.

In this paper, we use the port-Hamiltonian framework to describe the control problem of Circular Restricted Three-Body Problem (CRTBP), where the nonlinear dynamics are preserved. Then we use the energy-shaping and dissipation injection approach to shape the closed-loop Hamiltonian as the candidate of Lyapunov function. This allows us to stabilize the Lagrange points, which are originally unstable. These results provide a guidance for spacecraft missions to Lagrange points. In Section 2, we briefly summarize the Lagrange points in the CRTBP, while Section 3 describes the stabilization strategy using port-Hamiltonian approach. Results are discussed in Section 4, and Section 5 concludes this paper.

2. Lagrange points in the circular restricted three-body problem

In the Circular Restricted Three-Body Problem (CRTBP), two massive bodies move in a circular orbit around their common center of mass. The third mass is negligible with respect to the other two; thus, we neglect the force from the third mass acting on the other two larger ones. With respect to a rotating reference frame, the two co-orbiting bodies are considered stationary, and the ratios of mass and distance are considered instead of their actual values because their relative values are of the most importance. The governing equations of the planar circular restricted three-body problem [1] are:

$$\frac{d^2x}{dt^2} - 2\frac{dy}{dt} = x - (1-\mu)\frac{x+\mu}{r_1^3} - \mu\frac{x-1+\mu}{r_2^3} \tag{2}$$

$$\frac{d^2y}{dt^2} + 2\frac{dx}{dt} = y - (1-\mu)\frac{y}{r_1^3} - \mu\frac{y}{r_2^3}, \tag{3}$$

Table 1
Lagrange points for the Earth-Moon CRTBP with $\mu = 0.012155085$.

	L_1	L_2	L_3	L_4	L_5
x	0.836893	1.155699	−1.005065	$\frac{1}{2} - \mu$	$\frac{1}{2} - \mu$
y	0	0	0	$\frac{\sqrt{3}}{2}$	$\frac{-\sqrt{3}}{2}$

where x, y are position parallel and perpendicular to the line of two larger bodies, respectively. The r_1 and r_2 in the above equations,

$$r_1 = \sqrt{(x+\mu)^2 + y^2} \tag{4}$$

$$r_2 = \sqrt{(x-1+\mu)^2 + y^2}, \tag{5}$$

represent the distance from the third body to the two other larger bodies, which are located at $(-\mu, 0)$ and $(1-\mu, 0)$, respectively. In this paper, we set $\mu = 0.012155085$, which is the mass ratio in the Earth-Moon system.

It is demonstrated by Lagrange [1] that there are five equilibrium points for the third body in this system. These equilibrium points come from a balance in the centrifugal force and the gravitational attraction of the larger bodies, and they are now known as Lagrange points, or libration points [33]. The L_1, L_2, and L_3 Lagrange points can be obtained from solving algebraic equations:

$$x - (1-\mu)\frac{x+\mu}{r_1^3} - \mu\frac{x-1+\mu}{r_2^3} = 0 \tag{6}$$

$$y = 0, \tag{7}$$

while L_4 and L_5 each form an equilateral triangle with the centers of the large bodies. For the μ value discussed in this paper, we obtain the corresponding Lagrange points as summarized in Table 1.

Although the L_1, L_2, and L_3 points are unstable through linear stability analysis, there are periodic orbits called 'halo' orbits around these points in a three-body system [14,15]. These periodic halo orbits are what most of the Lagrange point space missions have used until now. Although they are not perfectly stable, a modest effort of station keeping [16–18] keeps a spacecraft in a desired Halo orbit obtained from the linearized CRTBP for a long time. For example, the earliest Lagrange point mission of 1978, the International Sun-Earth Explorer 3 (ISEE-3), was operated for four years in a halo orbit around the L_1 Sun-Earth Lagrange point with a maneuver required under 8.5 m/s/year [9,12]. Launched in 1997, the Advanced Composition Explorer (ACE) has fuel to orbit the L_1 Sun-Earth Lagrange point until 2024, with the maneuver required under 1.0 m/s/year [10,12].

3. Stabilization: port-Hamiltonian approach

The Jacobi integral is the only known conserved quantity for the circular restricted three-body problem. This integral is used to derive numerous solutions in special cases of the three-body problem and is expressed as follows in the (x, y) rotating coordinate system:

$$C = (x^2 + y^2) + 2\left(\frac{1-\mu}{r_1} + \frac{\mu}{r_2}\right) - (\dot{x}^2 + \dot{y}^2). \tag{8}$$

Here, we use the Hamiltonian:

$$H = -\frac{C}{2} = \frac{1}{2}(\dot{x}^2 + \dot{y}^2) - \frac{1}{2}\left[(x^2 + y^2) + 2\left(\frac{1-\mu}{r_1} + \frac{\mu}{r_2}\right)\right], \tag{9}$$

in the form of the Jacobi integral to reformulate the CRTBP problem into the port-Hamiltonian system:

$$\frac{d}{dt}\boldsymbol{x} = [\boldsymbol{J} - \boldsymbol{R}]\nabla_{\boldsymbol{x}} H + \boldsymbol{B}\boldsymbol{u}. \tag{10}$$

$\boldsymbol{x} = \begin{bmatrix} x & y & \dot{x} & \dot{y} \end{bmatrix}^T$ are state variables, and $\boldsymbol{u} = \begin{bmatrix} u_x & u_y \end{bmatrix}^T$ are inputs, which represent the thrust force acting on x and y directions. These inputs may be related to the state variables $\boldsymbol{x}$, which represent the state feedback control. $\boldsymbol{B} = \begin{bmatrix} 0 & 0 & 1 & 0 \\ 0 & 0 & 0 & 1 \end{bmatrix}^T$ is the matrix that maps the inputs to the state variables. $\boldsymbol{J}$ is a skew-symmetric matrix, which represents the energy (Hamiltonian) conserving part, and $\boldsymbol{R}$ is a symmetric positive semi-definite matrix, which represents the energy dissipation:

$$\boldsymbol{J} = \begin{bmatrix} 0 & 0 & 1 & 0 \\ 0 & 0 & 0 & 1 \\ -1 & 0 & 0 & 2 \\ 0 & -1 & -2 & 0 \end{bmatrix}, \quad \boldsymbol{R} = \boldsymbol{0}_{4\times 4}. \tag{11}$$

The zero matrix $\boldsymbol{R}$ comes from the fact that the CRTBP does not take account of any factors representing energy dissipation, such as the air drag. This renders the conservation of the Hamiltonian (Jacobi integral), which represents the energy in synodic coordinates. If we do not provide any input $\boldsymbol{u}$ to the system, the open-loop Hamiltonian $H(\boldsymbol{x})$ evolves as:

$$\begin{aligned} \frac{dH(\boldsymbol{x})}{dt} &= \nabla_{\boldsymbol{x}} H(\boldsymbol{x}) \cdot \frac{d\boldsymbol{x}}{dt} = \nabla_{\boldsymbol{x}} H(\boldsymbol{x}) \cdot [\boldsymbol{J} - \boldsymbol{R}] \nabla_{\boldsymbol{x}} H(\boldsymbol{x}) \\ &= \nabla_{\boldsymbol{x}} H(\boldsymbol{x}) \cdot [-\boldsymbol{R}] \nabla_{\boldsymbol{x}} H(\boldsymbol{x}) = 0, \end{aligned} \tag{12}$$

considering the $\boldsymbol{J}$ and $\boldsymbol{R}$ matrices defined above. Actually, the zero $\boldsymbol{R} = \boldsymbol{0}$ dissipation matrix and the zero input $\boldsymbol{u} = \boldsymbol{0}$ result in the same description as Hamiltonian mechanics if we define the Poisson bracket using $\boldsymbol{J}$: $\{F, G\}(\boldsymbol{x}) := \nabla_x F(\boldsymbol{x}) \cdot \boldsymbol{J} \nabla_x G(\boldsymbol{x})$ assuming the validity of the Jacobi identity; i.e., $\{F, \{G, K\}\} + \{G, \{K, F\}\} + \{K, \{F, G\}\} = 0$. The reformulation of the CRTBP into the port-Hamiltonian system paves the way for the following stabilization of Lagrange points based on the energy shaping and the dissipation injection.

3.1. Energy shaping

The Jacobi integral plays an important role in circular restricted three-body problems. It is highly related to the zero velocity curves, which reveal the regions to which the third body cannot be outside. This idea is also used to implement the reduced order nonlinear control on the orbit transfer from the Earth to the Moon, which focuses on controlling the Jacobi integral (Hamiltonian) [34]. Here, the goal of control is not to control the Hamiltonian, but to *shape* the Hamiltonian (energy) where the designed equilibrium points $\boldsymbol{x}^* = \begin{bmatrix} x^* & y^* & 0 & 0 \end{bmatrix}^T$ are stable. Thus, we design a closed-loop Hamiltonian $H_d(\boldsymbol{x})$ with the minimal position:

$$\boldsymbol{x}^* = \arg\min\{\boldsymbol{H}_d(\boldsymbol{x})\}. \tag{13}$$

Assuming the closed-loop system is also a port-Hamiltonian system, we have:

$$\frac{d\boldsymbol{x}}{dt} = [\boldsymbol{J} - \boldsymbol{R}] \nabla_{\boldsymbol{x}} H_d. \tag{14}$$

Comparing equation (14) with (10), we have the state feedback control law as $\boldsymbol{B}$ is full column rank but not full row rank:

$$\boldsymbol{u}_{ES}(\boldsymbol{x}) = (\boldsymbol{B}^T \boldsymbol{B})^{-1} \boldsymbol{B}^T [\boldsymbol{J} - \boldsymbol{R}] \nabla_{\boldsymbol{x}} H_a(\boldsymbol{x}) \tag{15}$$

$$H_a(\boldsymbol{x}) = H_d(\boldsymbol{x}) - H(\boldsymbol{x}), \tag{16}$$

and the difference between the closed-loop Hamiltonian and the open-loop Hamiltonian should satisfy:

$$\begin{bmatrix} \boldsymbol{B}^{\perp} [\boldsymbol{J} - \boldsymbol{R}] \\ \boldsymbol{B}^T \end{bmatrix} \nabla_{\boldsymbol{x}} H_a(\boldsymbol{x}) = 0, \tag{17}$$

where $\boldsymbol{B}^{\perp}$ is a left-annihilator of $\boldsymbol{B}$; i.e., $\boldsymbol{B}^{\perp} \boldsymbol{B} = \boldsymbol{0}$ of maximal rank.

For the circular restricted three-body problem, we design the closed-loop Hamiltonian as:

$$H_d(\boldsymbol{x}) = \frac{1}{2}[\dot{x}^2 + \dot{y}^2 + (x - x^*)^2 + (y - y^*)^2], \tag{18}$$

which has $\boldsymbol{x}^* = \begin{bmatrix} x^* & y^* & 0 & 0 \end{bmatrix}^T$ as the minimal point. This gives:

$$\begin{aligned} H_a(\boldsymbol{x}) = H_d(\boldsymbol{x}) - H(\boldsymbol{x}) &= \frac{1}{2}[(x^2 + y^2) + 2(\frac{1-\mu}{r_1} + \frac{\mu}{r_2})] \\ &+ \frac{1}{2}(x - x^*)^2 + \frac{1}{2}(x - x^*)^2, \end{aligned} \tag{19}$$

and it can be verified that $H_a(\boldsymbol{x})$ satisfies requirements in equation (17). According to equation (15), we obtain the state feedback control law for energy shaping:

$$\boldsymbol{u}_{ES}(\boldsymbol{x}) = (\boldsymbol{B}^T \boldsymbol{B})^{-1} \boldsymbol{B}^T [\boldsymbol{J} - \boldsymbol{R}] \nabla_{\boldsymbol{x}} H_a(\boldsymbol{x}) \tag{20}$$

$$= \begin{bmatrix} -\frac{\partial H_a}{\partial x} & -\frac{\partial H_a}{\partial y} \end{bmatrix}^T. \tag{21}$$

Under this control law, it can be shown that the closed-loop Hamiltonian is a Lyapunov function satisfying:

$$\begin{aligned} &H_d(\boldsymbol{x}) = 0, \ \ \boldsymbol{x} = \boldsymbol{x}^* \\ &H_d(\boldsymbol{x}) > 0, \ \ \forall \boldsymbol{x} \neq \boldsymbol{x}^* \\ &\frac{dH_d(\boldsymbol{x})}{dt} = \nabla_{\boldsymbol{x}} H_d(\boldsymbol{x}) \cdot [-\boldsymbol{R}] \nabla_{\boldsymbol{x}} H_d(\boldsymbol{x}) = 0, \ \ \forall \boldsymbol{x} \neq \boldsymbol{x}^*. \end{aligned} \tag{22}$$

According to Lyapunov stability theorem in equation (1), the equilibrium $\boldsymbol{x}^*$ of the closed-loop system is stable.

3.2. Dissipation injection

The previous energy shaping process utilizes a state feedback control law to shape the closed-loop Hamiltonian (energy) with a stable equilibrium at $\boldsymbol{x}^*$. However, the closed-loop Hamiltonian also remains a constant; i.e., $\frac{dH_d}{dt} = \nabla_{\boldsymbol{x}} H_d(\boldsymbol{x}) \cdot [-\boldsymbol{R}] \nabla_{\boldsymbol{x}} H_d(\boldsymbol{x}) = 0$. We may also design the equilibrium point as *asymptotically* stable. This can be achieved through dissipation injection, which modifies the $\boldsymbol{R}$ matrix in the closed-loop system. Aside from the energy shaping control law, we also implement a state feedback control representing dissipation injection:

$$\boldsymbol{u}_{DI}(x) = -\boldsymbol{K}_d \boldsymbol{B}^T \nabla_{\boldsymbol{x}} H_d(\boldsymbol{x}), \tag{23}$$

where $\boldsymbol{K}_d$ is positive definite. With $\boldsymbol{u}(\boldsymbol{x}) = \boldsymbol{u}_{ES}(\boldsymbol{x}) + \boldsymbol{u}_{DI}(\boldsymbol{x})$, we have the closed-loop system as:

$$\frac{d\boldsymbol{x}}{dt} = [\boldsymbol{J} - \boldsymbol{R}_d] \nabla_{\boldsymbol{x}} H_d, \tag{24}$$

with a closed-loop dissipation matrix: $\boldsymbol{R}_d(\boldsymbol{x}) = \boldsymbol{R}(\boldsymbol{x}) + \boldsymbol{B}(\boldsymbol{x}) \boldsymbol{K}_d \boldsymbol{B}^T$.

Thus, the closed-loop Hamiltonian evolves like:

$$\frac{dH_d}{dt} = \nabla_{\boldsymbol{x}} H_d(\boldsymbol{x}) \cdot [-\boldsymbol{R}_d] \nabla_{\boldsymbol{x}} H_d(\boldsymbol{x}) \leq 0, \ \ \forall \boldsymbol{x} \neq \boldsymbol{x}^*. \tag{25}$$

The closed-loop Hamiltonian $H_d(\boldsymbol{x})$ also satisfies $H_d(\boldsymbol{x}) = 0$, $\boldsymbol{x} = \boldsymbol{x}^*$ and $H_d(\boldsymbol{x}) > 0$, $\forall \boldsymbol{x} \neq \boldsymbol{x}^*$. As the union of complete trajectories contained entirely in the set $\mathcal{I} = \{\boldsymbol{x} | \frac{dH_d(\boldsymbol{x})}{dt} = 0\}$ has no trajectory except the trivial one $\boldsymbol{x}(t) = \boldsymbol{x}^*$ for $t \geq 0$, we obtain the *asymptotic* stability of the closed-loop system according to LaSalle's invariance principle [35], which generalized the Lyapunov stability theorem in equation (1).

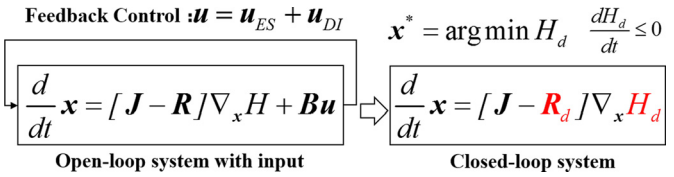

Fig. 1. Summary of the stabilization using the port-Hamiltonian approach, including energy shaping and dissipation injection.

The above framework of energy shaping and dissipation injection are summarized as Fig. 1, and an illustrative example of the duffing oscillator is provided in the Appendix A.

4. Results and discussion

In this section, we present the simulation results using the framework described before. The initial conditions are set as $\boldsymbol{x}_0 = \begin{bmatrix}0.5 & 0 & 0 & 0.2\end{bmatrix}^T$, and the dissipation injection matrix is set as $\boldsymbol{K}_d = \boldsymbol{I}_{2\times 2}$. The time integration is performed using explicit 4th order Runge-Kutta method with time step $\Delta t = 0.01$. In Fig. 2, we depict the orbits of the third body with a state feedback control $\boldsymbol{u} = \boldsymbol{u}_{ES} + \boldsymbol{u}_{DI}$ (the colored lines) compared with the uncontrolled system (the black solid lines). The equilibrium points $\boldsymbol{x}^*$ of H_d are set as L_1, L_2, L_3, L_4, and L_5 Lagrange points, respectively.

The results in Fig. 2 show that under control $\boldsymbol{u} = \boldsymbol{u}_{ES} + \boldsymbol{u}_{DI}$, the third body is enforced to fly to the designed Lagrange points and the Lagrange points are asymptotically stable in the controlled system. Fig. 3 shows the time history of inputs u_x and u_y according to the designed control law $\boldsymbol{u} = \boldsymbol{u}_{ES} + \boldsymbol{u}_{DI}$. As the third body approaches the designed Lagrange point, the inputs u_x and u_y tend toward zero, which indicates that no thrust force is required if the third body is not perturbed. Moreover, several highlights of the current framework are noteworthy:

Global stability: The linear stability analysis based on the linearized three-body equations only guarantees that the system is stable to infinitesimal perturbations, but it may be unstable to finite perturbations. Perturbations for the Earth-Moon Lagrange point missions under the CRTBP model include the eccentricity of the Earth-Moon orbit, the gravity from the other bodies [20], and the solar radiation pressure, among others. For the Sun-Earth Lagrange points mission, the perturbation from the gravity of the Moon is critical. Thus, the control strategy aimed at maintaining Halo orbits around a Lagrange point is only valid at a local region. Here, the stability is built based on Lyapunov's second stability method [21], which takes nonlinear dynamics into account and ensures global stability within the application region of the CRTBP model. These results in Fig. 2 reveal that we can start at the position that is far away from the designed Lagrange points. Particularly, if we modify the initial conditions as a random value in our numerical simulation, the third body will also fly to the designed Lagrange points as shown on the left of Fig. 4.

Arbitrary equilibrium position: In this paper, we initially limit our scope to the stabilization of the L_1, L_2, L_3, L_4, and L_5 Lagrange points, which are of the most interest for scientific and engineering applications [7,8,11]. However, the current framework can be further generalized to design control strategy for arbitrary equilibrium positions within the application region of the CRTBP model. For example, on the right of Fig. 4, we modify the designed equilibrium position as a random value (the red cross), and the third body also flies to this position according to our control law.

Stability against error in the thrusts: Here, we investigate the stability against perturbations in thrust force by adding the δ correlated Gaussian white noise $\boldsymbol{n}$ with a standard deviation of 0.4 in the thrust force $\boldsymbol{u}$. This noise serves as the model of the uncertainty of actuators and measurements as well as other possible

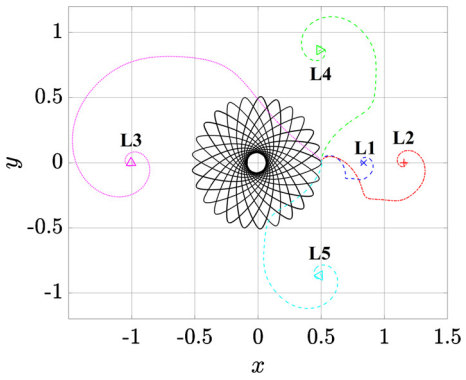

Fig. 2. The black solid line: the orbit of the third body without control. Colored lines: the orbit of the third body with state feedback control $\boldsymbol{u} = \boldsymbol{u}_{ES} + \boldsymbol{u}_{DI}$ targeting at different Lagrange points as the equilibrium $\boldsymbol{x}^*$: the blue dashed line: L_1; the red dashed dotted line: L_2; the magenta dotted line: L_3; the green dashed line: L_4; and the cyan dashed line: L_5. (For interpretation of the colors in the figure(s), the reader is referred to the web version of this article.)

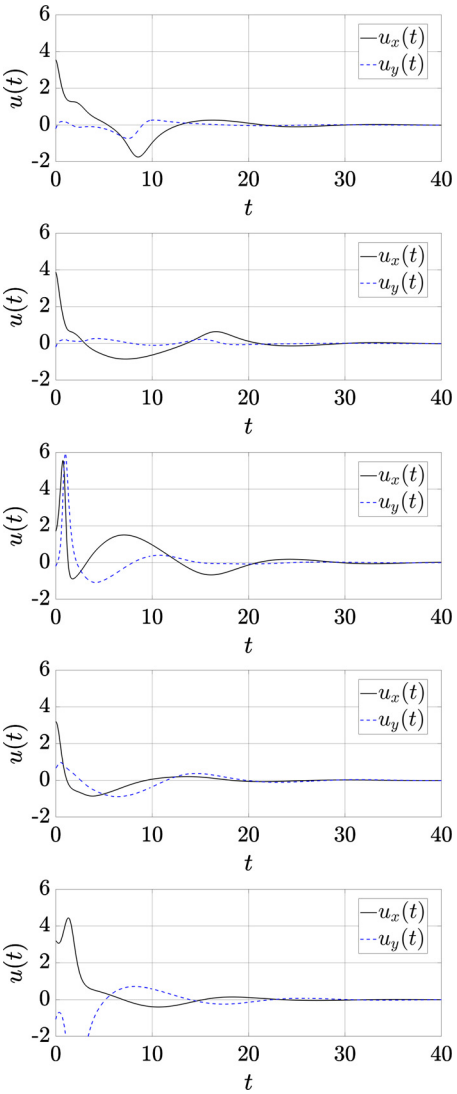

Fig. 3. Corresponding inputs u_x and u_y to stabilize the third body at Lagrange points. From top to bottom: $\boldsymbol{x}^*$ is set as L_1, L_2, L_3, L_4, and L_5, respectively.

perturbations; e.g., gravity from other bodies. We perform the simulation in three stages. In the first stage $t \in [0, 30]$, the third body starts with the same initial conditions of $\boldsymbol{x}_0 = \begin{bmatrix}0.5 & 0 & 0 & 0.2\end{bmatrix}^T$

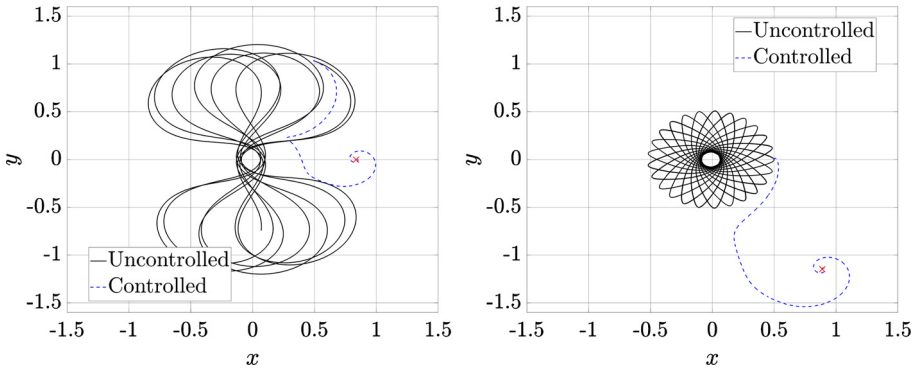

Fig. 4. Left: the orbit of the third body with state feedback control $\boldsymbol{u} = \boldsymbol{u}_{ES} + \boldsymbol{u}_{DI}$ compared with the uncontrolled system. The initial conditions are randomly generated, and the equilibrium point $\boldsymbol{x}^*$ is set as the L_1 Lagrange point. Right: the orbit of the third body with state feedback control $\boldsymbol{u} = \boldsymbol{u}_{ES} + \boldsymbol{u}_{DI}$ compared with the uncontrolled system. The initial conditions are $\boldsymbol{x}_0 = \begin{bmatrix} 0.5 & 0 & 0 & 0.2 \end{bmatrix}^T$, and the equilibrium point $\boldsymbol{x}^*$ is randomly generated.

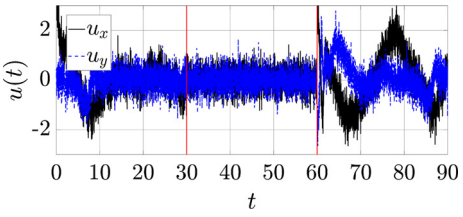

Fig. 5. The time history of the thrust force acting on the third body $\boldsymbol{u} = \boldsymbol{u}_{ES} + \boldsymbol{u}_{DI} + \boldsymbol{n}$ at stages $t \in [0, 30]$ and $t \in (60, 90]$. In $t \in (30, 60]$, the state feedback control is removed, and only noise exists in the thrust force; i.e., $\boldsymbol{u} = \boldsymbol{n}$.

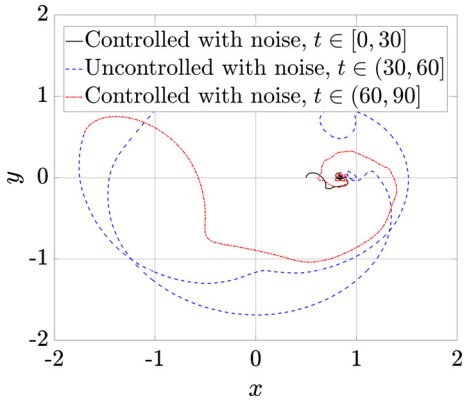

Fig. 6. The orbit of the third body illustrating the stability against noise in the thrust force. The black solid line: $t \in [0, 30]$, controlled by the state feedback with Gaussian white noise of the thrust force $\boldsymbol{u} = \boldsymbol{u}_{ES} + \boldsymbol{u}_{DI} + \boldsymbol{n}$; the blue dashed line: $t \in (30, 60]$, the uncontrolled system perturbed by Gaussian white noise of the thrust force $\boldsymbol{u} = \boldsymbol{n}$; and the red dashed dotted line: $t \in (60, 90]$, controlled by the state feedback with Gaussian white noise of the thrust force $\boldsymbol{u} = \boldsymbol{u}_{ES} + \boldsymbol{u}_{DI} + \boldsymbol{n}$. The equilibrium point $\boldsymbol{x}^*$ is set as the L_1 Lagrange point (the red triangle).

as used in Fig. 2. We implement the state feedback control designed in this paper with noise; i.e., $\boldsymbol{u} = \boldsymbol{u}_{ES} + \boldsymbol{u}_{DI} + \boldsymbol{n}$. In the next stage $t \in (30, 60]$, only noise exists in the thrust force $\boldsymbol{u} = \boldsymbol{n}$, which represents the perturbation on the third body. Finally, at $t \in (60, 90]$, we re-implement the state feedback control designed in this paper with noise; i.e., $\boldsymbol{u} = \boldsymbol{u}_{ES} + \boldsymbol{u}_{DI} + \boldsymbol{n}$. The equilibrium position is set as the first Lagrange point L_1, and the thrust force acting on the third body in this simulation is illustrated in Fig. 5. The orbit of the third body in Fig. 6 and the time history of the $x - y$ positions in Fig. 7 reveal that the control law designed here also works even though the Gaussian white noise is introduced in the thrust force, which indicates that this control law is stable against error in the thrust force.

Superiority over a linear controller: Furthermore, at $t \in (30, 60]$, the third body is perturbed by the noise $\boldsymbol{u} = \boldsymbol{n}$ and moves to the

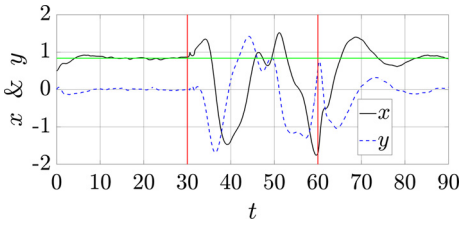

Fig. 7. Time history of x and y positions for the third body. The black solid line: the x position; the blue dashed line: the y position; and the green horizontal line: $x^* = 0.836893$, which is the equilibrium position in this case; i.e., the first Lagrange point L_1. The two red lines represent $t = 30$ and $t = 60$ when we remove and add the state feedback control $\boldsymbol{u} = \boldsymbol{u}_{ES} + \boldsymbol{u}_{DI}$, respectively. The Gaussian white noise of the thrust force exists for $t \in [0, 90]$.

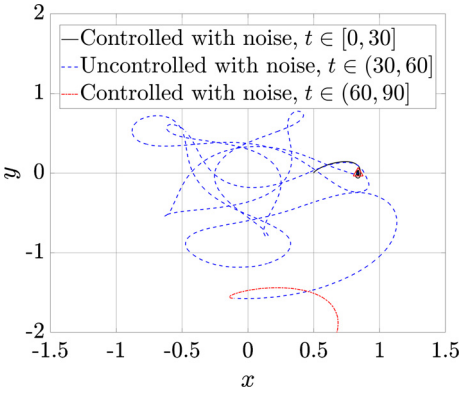

Fig. 8. The orbit of the third body illustrating the failure of a linear controller. The black solid line: $t \in [0, 30]$, controlled by the state feedback with Gaussian white noise of the thrust force $\boldsymbol{u} = \boldsymbol{u}_{LQR} + \boldsymbol{n}$; the blue dashed line: $t \in (30, 60]$, the uncontrolled system perturbed by Gaussian white noise of the thrust force $\boldsymbol{u} = \boldsymbol{n}$; and the red dashed dotted line: $t \in (60, 90]$, controlled by the state feedback with Gaussian white noise of the thrust force $\boldsymbol{u} = \boldsymbol{u}_{LQR} + \boldsymbol{n}$. The equilibrium point $\boldsymbol{x}^*$ is set as the L_1 Lagrange point (the red triangle).

region far away from the equilibrium point L_1, where the dynamics linearized around L_1 and the linear controller based on this may fail. To illustrate, we implement the same Gaussian white noise but utilize the Linear Quadratic Regulator controller [16,36,37] according to the CRTBP linearized around the L_1 Lagrange point: $\frac{d\boldsymbol{x}}{dt} = \boldsymbol{A}\boldsymbol{x} + \boldsymbol{B}\boldsymbol{u}$, where $\boldsymbol{A}$ is the Jacobian of $(\boldsymbol{J} - \boldsymbol{R})\nabla H(\boldsymbol{x})$ evaluated at the equilibrium point $\boldsymbol{x}^*$; i.e. the first Lagrange point L_1 in this case. Using the Linear Quadratic Regulator (LQR) controller, we obtain the control law as $\boldsymbol{u}_{LQR} = -\boldsymbol{K}(\boldsymbol{x} - \boldsymbol{x}^*)$, where $\boldsymbol{K} = \begin{bmatrix} 19.7962 & -2.8238 & 5.5648 & 1.6912 \\ 7.5052 & -0.9494 & 1.6912 & 1.7338 \end{bmatrix}$ minimizes the cost function $J_{LQR} = \int_0^\infty \boldsymbol{x}^T \boldsymbol{Q}\boldsymbol{x} + \boldsymbol{u}^T \boldsymbol{R}\boldsymbol{u}$ with $\boldsymbol{Q} = \boldsymbol{I}_{4\times4}$ and $\boldsymbol{R} = \boldsymbol{I}_{2\times2}$.

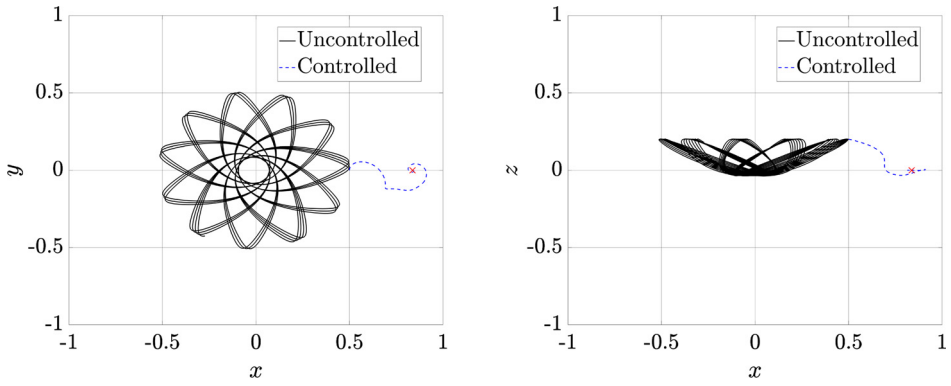

Fig. 9. The orbit of the third body in $x-y$ plane (left) and $y-z$ plane (right) with state feedback control $\boldsymbol{u}=\boldsymbol{u}_{ES}+\boldsymbol{u}_{DI}$ compared with the uncontrolled system. The equilibrium point $\boldsymbol{x}^*$ is set as the L_1 Lagrange point (the red cross).

This feedback gain $\boldsymbol{K}$ is obtained through solving the algebraic Riccati equation. In Fig. 8, the third body also starts from the same initial condition $\boldsymbol{x}_0$ with the same Gaussian white noise on the thrust force $\boldsymbol{n}$, but we implement the LQR controller $\boldsymbol{u}=\boldsymbol{u}_{LQR}$ here. Results at $t\in[0,30]$ indicate that the LQR controller is also able to stabilize the third body at the first Lagrange point L_1. In contrast to the results under control law $\boldsymbol{u}=\boldsymbol{u}_{ES}+\boldsymbol{u}_{DI}$ in Fig. 6, the third body cannot return back to the Lagrange point L_1 at $t\in(60,90]$ using LQR controller $\boldsymbol{u}_{LQR}$. These results indicate that after the perturbation in $t\in(30,60]$, the third body moves beyond the application range of a linear controller, and the nonlinear effects are critical. The control law designed in this paper retains the original nonlinear dynamics and still works when the third body is far away from the designed equilibrium point, which is demonstrated in the $t\in(60,90]$ stage in Figs. 6 and 7.

Extension to the 3D CRTBP: For ease of exposition in previous discussions, we restrict the motion and thrust on the $x-y$ plane. In fact, the current framework has the potential to be further extended to the three-dimensional CRTBP (3D CRTBP) by introducing dynamics and thrust in the z direction. Here, we also rewrite the 3D CRTBP into the port-Hamiltonian framework with the Hamiltonian proportional to the Jacobi integral in 3D CRTBP; i.e., $H=-\frac{C}{2}=\frac{1}{2}(\dot{x}^2+\dot{y}^2+\dot{z}^2)-\frac{1}{2}[(x^2+y^2)+2(\frac{1-\mu}{r_1}+\frac{\mu}{r_2})]$. Generalizing the state variables as $\boldsymbol{x}=\begin{bmatrix}x & y & z & \dot{x} & \dot{y} & \dot{z}\end{bmatrix}^T$ and inputs as $\boldsymbol{u}=\begin{bmatrix}u_x & u_y & u_z\end{bmatrix}^T$, we can rewrite the 3D CRTBP into the port-Hamiltonian description as equation (10) with:

$$\boldsymbol{J}=\begin{bmatrix}\boldsymbol{0}_{3\times3} & \boldsymbol{I}_{3\times3}\\ -\boldsymbol{I}_{3\times3} & \boldsymbol{G}\end{bmatrix},\ \boldsymbol{G}=\begin{bmatrix}0 & 2 & 0\\ -2 & 0 & 0\\ 0 & 0 & 0\end{bmatrix},$$
$$\boldsymbol{R}=\boldsymbol{0}_{6\times6},\ \boldsymbol{B}=\begin{bmatrix}\boldsymbol{0}_{3\times3} & \boldsymbol{I}_{3\times3}\end{bmatrix}^T. \tag{26}$$

Following the same procedure to design the state feedback control based on the energy shaping and dissipation injection, we obtain a similar control law, where the closed-loop Hamiltonian is designed as: $H_d(\boldsymbol{x})=\frac{1}{2}[\dot{x}^2+\dot{y}^2+\dot{z}^2+(x-x^*)^2+(y-y^*)^2+(z-z^*)^2]$. In Fig. 9, we show that the third body starts from an initial position outside of the $x-y$ plane $\boldsymbol{x}_0=\begin{bmatrix}0.5 & 0 & 0.2 & 0 & 0.2 & 0\end{bmatrix}^T$, and the designed equilibrium point is the L_1 Lagrange point. Results demonstrate that the proposed state feedback control law $\boldsymbol{u}=\boldsymbol{u}_{ES}+\boldsymbol{u}_{DI}$ has the potential to be generalized to the 3D CRTBP, where the closed-loop equilibrium point achieves asymptotic stability; i.e., it is stable to perturbations in x, y, and z directions.

5. Conclusion

In this paper, we use the port-Hamiltonian approach to reformulate the Circular Restricted Three-Body Problem (CRTBP) with input, which preserves the original nonlinear dynamics. The Hamiltonian is thus a natural candidate of Lyapunov function. Through shaping the closed-loop Hamiltonian (energy), we stabilize the closed-loop system at a designed equilibrium position. With further dissipation injection, the designed equilibrium point is asymptotically stable.

The control strategy designed here is then applied to the CRTBP and successfully stabilizes the Lagrange points, which are of the most scientific and engineering interest. Furthermore, the designed control approach shows global stability within the application region of the CRTBP model, which indicates that the third body with arbitrary initial condition will fly to the designed position. This model is also applicable to a set arbitrary equilibrium point. Moreover, the current framework is also stable against error in the thrust, which is modeled as Gaussian white noise. Compared with the Linear Quadratic Regulator (LQR), the nonlinear controller designed here still works when the third body moves beyond the region of applicability of the linearized dynamics, where the linear controller may fail. At last, this framework has the potential to be generalized to the three-dimensional Circular Restricted Three-Body Problem (3D CRTBP), where both the perturbation and the thrust out of plane are included in the model.

Appendix A. An illustrative example: the duffing oscillator

Here, we illustrate the basic idea of the proposed framework using the duffing oscillator:

$$\ddot{x}+\delta\dot{x}+\alpha x+\beta x^3=u. \tag{A.1}$$

The undamped ($\delta=0$) open-loop ($u=0$) duffing oscillator is a Hamiltonian system with:

$$H(\boldsymbol{x})=\frac{1}{2}\dot{x}^2+\frac{1}{2}\alpha x^2+\frac{1}{4}\beta x^4. \tag{A.2}$$

The damped duffing system with input can be written as the port-Hamiltonian system:

$$\frac{d}{dt}\boldsymbol{x}=[\boldsymbol{J}-\boldsymbol{R}]\nabla_{\boldsymbol{x}}H(\boldsymbol{x})+\boldsymbol{B}u. \tag{A.3}$$

$\boldsymbol{x}=\begin{bmatrix}x & \dot{x}\end{bmatrix}^T$ are state variables and u is the input. $\boldsymbol{B}=\begin{bmatrix}0 & 1\end{bmatrix}^T$ maps the input to the state variables. The skew-symmetric matrix is $\boldsymbol{J}=\begin{bmatrix}0 & 1\\ -1 & 0\end{bmatrix}$, and the symmetric positive semi-definite matrix is $\boldsymbol{R}=\begin{bmatrix}0 & 0\\ 0 & \delta\end{bmatrix}$. The coefficients are set as $\alpha=1$, $\beta=-1$, and the initial conditions are set as $\boldsymbol{x}=\begin{bmatrix}0.5 & 0.5\end{bmatrix}^T$. Under these parameters, the equilibrium point of the duffing oscillator $x=0$ is

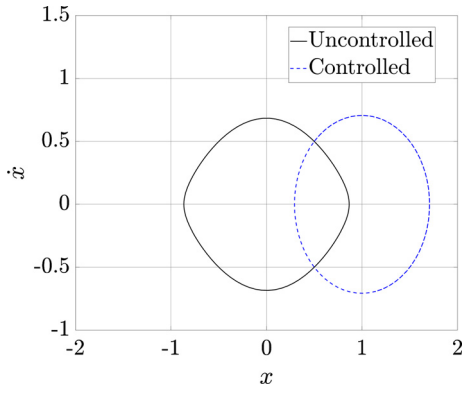

Fig. A.10. The $x-\dot{x}$ plane for the undamped duffing oscillator with state feedback control $\boldsymbol{u}=\boldsymbol{u}_{ES}$ compared with the uncontrolled system.

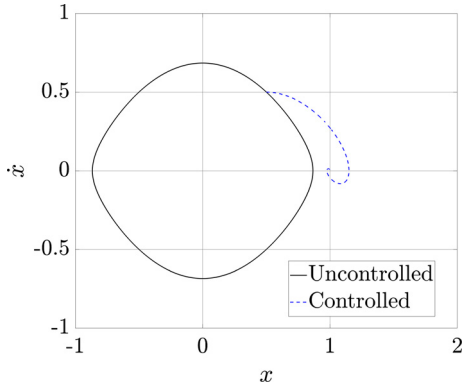

Fig. A.11. The $x-\dot{x}$ plane for the undamped duffing oscillator with state feedback control $\boldsymbol{u}=\boldsymbol{u}_{ES}+\boldsymbol{u}_{DI}$ compared with the uncontrolled system.

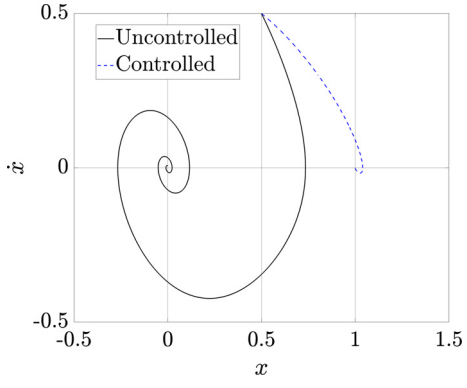

Fig. A.12. The $x-\dot{x}$ plane for the damped duffing oscillator with state feedback control $\boldsymbol{u}=\boldsymbol{u}_{ES}$ compared with the uncontrolled system.

stable, while equilibrium points $x=\pm\sqrt{-\frac{\alpha}{\beta}}$ are unstable. We now consider the undamped duffing oscillator with control. The closed-loop Hamiltonian is designed as:

$$H_d(\boldsymbol{x})=\frac{1}{2}\dot{x}^2+\frac{1}{2}(x-x^*)^2, \tag{A.4}$$

which reaches its minimal value at the equilibrium point $\boldsymbol{x}=\begin{bmatrix}x^* & 0\end{bmatrix}^T$. In this example, we set $x^*=1$. We implement the energy shaping control $\boldsymbol{u}_{ES}$ according to equation (15):

$$u_{ES}=\alpha x+\beta x^3-(x-x^*). \tag{A.5}$$

The phase planes of the controlled and uncontrolled systems are shown in Fig. A.10. Then, we implement the dissipation injection to this undamped system to make the equilibrium point asymptotically stable. Using equation (23) with $K_d=1$, we obtain:

$$u_{DI}=-\dot{x}. \tag{A.6}$$

With both the energy shaping and dissipation injection $u=u_{ES}+u_{DI}$, the controlled system reaches the designed equilibrium point as shown in Fig. A.11. Finally, we implement the energy shaping control law $u=u_{ES}$ only on the damped duffing oscillator with $\delta=1$. Results in Fig. A.12 show that the proposed control law also works even when the original system is dissipative. Actually, we do not need the dissipation injection step to make the equilibrium point asymptotically stable if the original system already has dissipation.

References

[1] Z. Musielak, B. Quarles, The three-body problem, Rep. Prog. Phys. 77 (6) (2014) 065901.
[2] F. Dubeibe, F. Lora-Clavijo, G.A. González, Pseudo-Newtonian planar circular restricted 3-body problem, Phys. Lett. A 381 (6) (2017) 563–567.
[3] G.W. Hill, On the part of the motion of the lunar perigee which is a function of the mean motions of the sun and moon, Acta Math. 8 (1) (1886) 1–36.
[4] B. Gladman, Dynamics of systems of two close planets, Icarus 106 (1) (1993) 247–263.
[5] S. Satyal, B. Quarles, T. Hinse, Application of chaos indicators in the study of dynamics of s-type extrasolar planets in stellar binaries, Mon. Not. R. Astron. Soc. 433 (3) (2013) 2215–2225.
[6] F. Szenkovits, Z. Makó, About the hill stability of extrasolar planets in stellar binary systems, Celest. Mech. Dyn. Astron. 101 (3) (2008) 273–287.
[7] G. Pilbratt, J. Riedinger, T. Passvogel, G. Crone, D. Doyle, U. Gageur, A. Heras, C. Jewell, L. Metcalfe, S. Ott, et al., Herschel space observatory-an esa facility for far-infrared and submillimetre astronomy, Astron. Astrophys. 518 (2010) L1.
[8] J.P. Gardner, J.C. Mather, M. Clampin, R. Doyon, M.A. Greenhouse, H.B. Hammel, J.B. Hutchings, P. Jakobsen, S.J. Lilly, K.S. Long, et al., The James Webb space telescope, Space Sci. Rev. 123 (4) (2006) 485–606.
[9] R. Farquhar, The flight of ISEE-3/ICE-origins, mission history, and a legacy, in: AIAA/AAS Astrodynamics Specialist Conference and Exhibit, 1998, p. 4464.
[10] E.C. Stone, A. Frandsen, R. Mewaldt, E. Christian, D. Margolies, J. Ormes, F. Snow, The advanced composition explorer, Space Sci. Rev. 86 (1–4) (1998) 1–22.
[11] T.H. Sweetser, S.B. Broschart, V. Angelopoulos, G.J. Whiffen, D.C. Folta, M.-K. Chung, S.J. Hatch, M.A. Woodard, Artemis mission design, in: The ARTEMIS Mission, Springer, 2012, pp. 61–91.
[12] M. Shirobokov, S. Trofimov, M. Ovchinnikov, Survey of station-keeping techniques for libration point orbits, J. Guid. Control Dyn. 40 (5) (2017) 1085–1105.
[13] K. Meyer, D. Schmidt, The stability of the Lagrange triangular point and a theorem of Arnold, J. Differ. Equ. 62 (2) (1986) 222–236.
[14] G. Gómez, A. Jorba, J. Masdemont, C. Simó, Study of the transfer from the Earth to a halo orbit around the equilibrium point L_1, Celest. Mech. Dyn. Astron. 56 (4) (1993) 541–562.
[15] D.L. Richardson, Halo orbit formulation for the isee-3 mission, J. Guid. Control Dyn. 3 (6) (1980) 543–548.
[16] D. Cielaszyk, B. Wie, New approach to halo orbit determination and control, J. Guid. Control Dyn. 19 (2) (1996) 266–273.
[17] J. Ardaens, S. D'Amico, Control of formation flying spacecraft at a Lagrange point, No. 00-08.
[18] X. Ming, X. Shijie, Trajectory and correction maneuver during the transfer from Earth to halo orbit, Chin. J. Aeronaut. 21 (3) (2008) 200–206.
[19] Y. Akiyama, M. Bando, S. Hokamoto, Explicit form of station-keeping and formation flying controller for libration point orbits, J. Guid. Control Dyn. 41 (6) (2018) 1407–1415.
[20] H. Yamato, D. Spencer, Transit-orbit search for planar restricted three-body problems with perturbations, J. Guid. Control Dyn. 27 (6) (2004) 1035–1045.
[21] A.M. Lyapunov, The general problem of the stability of motion, Int. J. Control 55 (3) (1992) 531–534.
[22] N.P. Bhatia, G.P. Szegö, Stability Theory of Dynamical Systems, Springer Science & Business Media, 2002.
[23] A. Yahalom, J. Levitan, M. Lewkowicz, L. Horwitz, Lyapunov vs. geometrical stability analysis of the Kepler and the restricted three body problems, Phys. Lett. A 375 (21) (2011) 2111–2117.
[24] M.S. De Queiroz, D.M. Dawson, S.P. Nagarkatti, F. Zhang, Lyapunov-Based Control of Mechanical Systems, Springer Science & Business Media, 2012.
[25] C.G. Jacobi, Sur le mouvement d'un point et sur un cas particulier du problème des trois corps, Comput. Rend. 3 (1836) 59–61.
[26] L. Euler, De motu rectilineo trium corporum se mutuo attrahentium, in: Novi Commentarii Academiae Scientarum Petropolitanae, vol. 11, 1767, pp. 144–151, in: Oeuvres, Seria Secunda, vol. 25, 1767, p. 286.

[27] A. van der Schaft, D. Jeltsema, et al., Port-Hamiltonian systems theory: an introductory overview, Found. Trends® Syst. Control 1 (2–3) (2014) 173–378.
[28] A.J. Van Der Schaft, J.M. Schumacher, An Introduction to Hybrid Dynamical Systems, vol. 251, Springer, London, 2000.
[29] R. Ortega, A.J. Van Der Schaft, I. Mareels, B. Maschke, Putting energy back in control, IEEE Control Syst. 21 (2) (2001) 18–33.
[30] R. Ortega, A. Van Der Schaft, B. Maschke, G. Escobar, Interconnection and damping assignment passivity-based control of port-controlled Hamiltonian systems, Automatica 38 (4) (2002) 585–596.
[31] R. Ortega, A. Van Der Schaft, F. Castanos, A. Astolfi, Control by interconnection and standard passivity-based control of port-Hamiltonian systems, IEEE Trans. Autom. Control 53 (11) (2008) 2527–2542.
[32] C. Liu, L. Dong, Physics-based control education: energy, dissipation and structure assignments, Eur. J. Phys. 40 (3) (2019) 035006, https://doi.org/10.1088/1361-6404/ab03e8.
[33] R.L. Jarabek, Investigation of Manifolds and Optimized Trajectories in the Three-Body Problem, Ph.D. thesis, 2004.
[34] C. Liu, L. Dong, Reduced order nonlinear control for circular restricted three-body problem: energy approach (under review).
[35] J. LaSalle, Some extensions of Liapunov's second method, IRE Trans. Circuit Theory 7 (4) (1960) 520–527.
[36] H. Kwakernaak, R. Sivan, Linear Optimal Control Systems, vol. 1, Wiley-Interscience, New York, 1972.
[37] K. Zhou, J.C. Doyle, K. Glover, et al., Robust and Optimal Control, vol. 40, Prentice Hall, New Jersey, 1996.